OXFORD

Cerebral Cortex, April 2021;31: 1970–1986

doi: 10.1093/cercor/bhaa334
Advance Access Publication Date: 30 November 2020
Original Article

ORIGINAL ARTICLE

Reconfiguration of Directed Functional Connectivity Among Neurocognitive Networks with Aging: Considering the Role of Thalamo-Cortical Interactions

Moumita Das[1,†], Vanshika Singh[1], Lucina Q. Uddin[2], Arpan Banerjee[1] and Dipanjan Roy[1,]

[1]Cognitive Brain Dynamics Lab National Brain Research Centre NH-8 Manesar Haryana-122 052, India and [2]Department of Psychology, University of Miami, Coral Gables, FL 33124, USA

Address correspondence to Dipanjan Roy, Cognitive Brain Dynamics Lab, National Brain Research Centre, NH 8, Manesar, Gurgaon 122052, India. Email: dipanjan.nbrc@gov.in.
[†]Current address: Department of applied statistics, Basque Center for Applied Mathematics, Bilbao 48009, Spain

Abstract

A complete picture of how subcortical nodes, such as the thalamus, exert directional influence on large-scale brain network interactions across age remains elusive. Using directed functional connectivity and weighted net causal outflow on resting-state fMRI data, we provide evidence of a comprehensive reorganization within and between neurocognitive networks (default mode: DMN, salience: SN, and central executive: CEN) associated with age and thalamocortical interactions. We hypothesize that thalamus subserves both modality-specific and integrative hub role in organizing causal weighted outflow among large-scale neurocognitive networks. To this end, we observe that within-network directed functional connectivity is driven by thalamus and progressively weakens with age. Secondly, we find that age-associated increase in between CEN- and DMN-directed functional connectivity is driven by both the SN and the thalamus. Furthermore, left and right thalami act as a causal integrative hub exhibiting substantial interactions with neurocognitive networks with aging and play a crucial role in reconfiguring network outflow. Notably, these results were largely replicated on an independent dataset of matched young and old individuals. Our findings strengthen the hypothesis that the thalamus is a key causal hub balancing both within- and between-network connectivity associated with age and maintenance of cognitive functioning with aging.

Key words: directed functional connectivity, healthy aging, multivariate Granger causality, salience network, thalamus, weighted net causal outflow

Introduction

In the last decade, there has been an enormous interest in studying the coordinated activity in distributed brain areas when individuals are engaged in internally driven tasks, such as meandering through self-referential thoughts while seemingly at rest, or more specifically not engaged in a state of goal directed action and perception (Bressler and Menon 2010; Deco et al. 2011; Raichle 2015). The functional organization (Bressler and Menon 2010) that dominates the landscape of both resting state and task activity has been broadly classified into three networks based on the correlation patterns estimated from BOLD time series signals. These networks are known as the default mode network (DMN)/medial frontoparietal network, salience network (SN)/midcingulo-insular network, and central executive network (CEN)/lateral frontoparietal network (Menon and Uddin 2010; Uddin et al. 2019). The DMN comprises posterior cingulate cortex (PCC), medial prefrontal cortex (MPFC), and lateral parietal cortices, and is implicated in self-referential

mental activities (Uddin et al. 2007, Buckner et al. 2008). The CEN comprises rostral and caudal bilateral middle frontal cortex (MFC) and bilateral superior parietal cortex (SPC), and is implicated in decision making and executive functions (Corbetta and Shulman 2002; Fox et al. 2006). The SN, which comprises bilateral anterior insula (AI) and caudal, rostral bilateral anterior cingulate cortices (ACC) is important for detection and mapping of salient inputs and routing these inputs to control areas for mediating cognitive control (Menon and Uddin 2010; Uddin 2015).

Interestingly, modification of interconnections within and between the DMN, CEN, SN is altered in a large number of psychiatric and neurological disorders, for instance, Alzheimer's disease, autism spectrum disorder, attention deficit/hyperactivity disorder, psychosis, and depression (Woodward and Cascio 2015; Abi-Dargham and Horga 2016). The SN, in addition to detecting salient stimuli, plays an important role in switching between the DMN and CEN in task conditions as well as in the resting state (Sridharan et al. 2008; Uddin et al. 2011). This enables rapid detection of goal-directed or goal-oriented salient events from the external environments and facilitation of access to appropriate cognitive resources towards internal oriented cognition. Secondly, dynamic functional interactions of the SN were among the most spatially varied in the brain. Third, SN nodes maintained a consistently high level of network centrality over time, indicating that this network is a hub for facilitating flexible cross-network interactions (Menon and Uddin 2010; Chen et al. 2016). With the anterior insula as its integral hub, the salience network assists target brain regions in the generation of appropriate behavioral responses to salient stimuli subserving externally driven and internally oriented control and attention (Menon and Uddin 2010; Uddin et al. 2011). During the performance of many tasks, correlation among the nodes of SN in tandem with CEN increases, while the corresponding correlation among the DMN nodes decreases.

An important caveat to all the resting brain network studies is that they mostly concentrate on cortical nodes and ignore the crucial influence of thalamocortical interactions on whole-brain network dynamics. The thalamus, a centrally located relay station for transmitting information throughout the brain, participates in communication with many associative brain regions and involves global multifunctional pathways. Incorporating 10 449 metastudies, Hwang et al. (2017) recently showed that the thalamus is engaged in multiple cognitive functions and is a critical integrative hub for functional brain networks. Cross-sectional studies of normal aging have also reported smaller thalamic volumes in older than younger adults (Cherubini et al. 2009; Hughes et al. 2012). Further, several recent studies have endeavored to unravel changes in the brain's structural and functional connectivity with aging and the cognitive implications of these changes. The vast majority of these studies have used spatial and temporal correlation across different brain regions as measure of functional connectivity to characterize age-related changes in brain's large-scale functional connectivity patterns (Vij et al. 2018). However, exactly how normal aging affects thalamic interconnections with other brain networks and its implication in cognitive changes are not completely understood, and thus warrant further investigation. From a methodological standpoint, if the thalamus acts as a common source to cortical inputs and also receives feedback from the cortex as proposed by theories such as thalamocortical dysryhtmia (Llinás et al. 1999; Vanneste et al. 2018), a causality analysis that ignores thalamocortical contribution to brain dynamics is of very limited scope, and possibly paints an inaccurate account of the underlying complexity. Thus, the primary goal of this study is to test our hypothesis of whether the thalamus acts as modality selective as well as an integrative hub in reorganizing both within and between-network causal outflow among major neurocognitive networks with age. Secondly, we hypothesize that the within network causal drive progressively weakens with age (young > old), however, the between-network drive increases with age (old > young). Finally, we conjecture that SN still remains at the apex of the hierarchy by selectively driving DMN and CEN in the absence of thalamocortical interactions, however, in the presence of such interactions, the thalamus proper (including first and second order thalamic nuclei combined) exhibits substantial-directed functional connectivity with DMN, CEN and causally drives these networks via SN which subserve role of a key mediator (connector hub) and facilitate increased internetwork interactions with age. Our findings may be a first step for an understanding more general interactions between key neurocognitive networks and subcortical structures to facilitate bidirectional causal information processing at the functional level.

Material and Methods

Participants

About 25 young and 24 elderly individuals participated in this study after providing written informed consent. The young group ranged in age from 18 to 33 years (mean age = 25.7 ±4 years, 13 female) and the elderly group ranged in age from 55 to 80 years (mean age = 67.99 ±9 years, 18 female). The study was performed under the compliance of laws and guidelines approved by the ethics committee of Charité University, Berlin. In the replication cohort, we identified a group of 24 young (age: 24.58 years; range: 18–31 years; 11 female) and 25 elderly participants (age: 64.8 years; range: 50–81 years; 18 female) from the publicly available Cambridge Aging Neuroscience dataset (https://camcan-archive.mrc-cbu.cam.ac.uk//dataaccess/) who were similar in mean age and gender distribution to the Berlin dataset.

Data Acquisition

Resting-state fMRI as well as diffusion weighted (dw) MRI data were collected from 49 healthy participants at the Charité University Berlin, Germany (Schirner et al. 2015). Each fMRI dataset amounts to 661 time points recorded at TR = 2 s, that is, about 22 min. In the same session, EEG was also recorded, but these data are not used for our current analysis. No other controlled task was performed. Resting-state BOLD activity was recorded while subjects were asked to stay awake with their eyes closed, using a 3 T Siemens Trim Trio scanner and a 12 channel Siemens head coil (voxel size). Structural (T1-weighted high-resolution three-dimensional MP-RAGE sequence; TR = 1900 ms, TE = 2.52 ms, TI = 900 ms, flip angle = 9°, field of view (FOV) = 256 mm × 256 mm × 192 mm, 256 × 256 × 192 Matrix, 1.0 mm isotropic voxel resolution), diffusion-weighted (T2-weighted sequence; TR = 7500 ms, TE = 86 ms, FOV = 192 mm × 192 mm, 96 × 96 Matrix, 61 slices, 2.3 mm isotropic voxel resolution, 64 diffusion directions), and fMRI data (2-dimensional T2-weighted gradient echo planar imaging blood oxygen level-dependent contrast sequence;

TR = 1940 ms, TE = 30 ms, flip angle = 78°, FOV = 192 mm × 192 mm, 3 mm × 3 mm voxel resolution, 3 mm slice thickness, 64 × 64 matrix, 33 slices, 0.51 ms echo spacing, 668 TRs, 7 initial images were acquired and discarded to allow magnetization to reach equilibrium; eyes-closed resting-state) were acquired on a 12-channel Siemens 3 Tesla Trio MRI scanner at the Berlin Center for Advanced Neuroimaging, Berlin, Germany.

Data Analysis

rs-fMRI Preprocessing

The major preprocessing steps applied to T1 anatomical images were skull stripping, removal of nonbrain tissue, brain mask generation, cortical reconstruction, motion correction, intensity normalization, white matter (WM) and subcortical segmentation, cortical tessellation generating GM–WM and GM–pia interface surface-triangulations, and probabilistic atlas-based cortical and subcortical parcellation. The parcellation used in this study is Desikan–Killiany parcellation (Desikan et al. 2006), which consists of 68 ROIs with 34 ROIs in each hemisphere and several first- and second-order thalamic nuclei is further aggregated into two thalamic regions known as right and left thalamus proper in Desikan–Killiany parcellation. For our present analysis along with 18 cortical regions anchored in three major neurocognitive networks (see details of node selection in the next subsection), two thalamic regions, left and right thalami were included based on this parcellation (in total 20 brain regions). The regional resting-state fMRI time series was computed for each of the regions-of-interest (ROIs, defined by the Desikan–Killiany atlas; Desikan et al. 2006, as implemented in FreeSurfer) by averaging all the voxels within each region at each time point in the time series.

These regional time series were temporally filtered using a bandpass filter ($0.01\ \text{Hz} < f < 0.08\ \text{Hz}$) (Li et al. 2015; Yuen et al. 2019). The empirical BOLD time series signals from ROIs used in this paper for the estimation of directed functional connectivity and weighted net causal flow were generated by using an automated pipeline as described in detail elsewhere (Schirner et al. 2015).

Selection of Brain Regions from Neurocognitive Networks

To identify RSN activity, a spatial Group ICA decomposition was performed for the fMRI data of all subjects using FSL MELODIC (Beckmann and Smith 2004; MELODIC v4.0; FMRIB Oxford University) with the following parameters: high pass filter cut off: 100 s, MCFLIRT motion correction, BET brain extraction, spatial smoothing, normalization to MNI152, temporal concatenation, dimensionality restriction to 30 output components. ICs that correspond to RSNs were automatically identified by spatial correlation with the 9 out of the 10 well-matched pairs of networks of the 29 671-subject Brain Map activation database as described in (Smith et al. 2009) (excluding the cerebellum network). Subsequently, the three key intrinsic neurocognitive networks were identified by spatially matching with pre-existing templates following widely accepted seven networks resting-state parcellation proposed by Buckner et al. (2011). Each of the cortical regions was classified further down to seven parcellated resting networks (Fig. 1).

In our subsequent analysis, we considered three resting-state networks, namely the DMN, SN, CEN (node details are provided in Table 1).

The selection of ROIs for the neurocognitive networks under investigation was partly data driven and partly literature based.

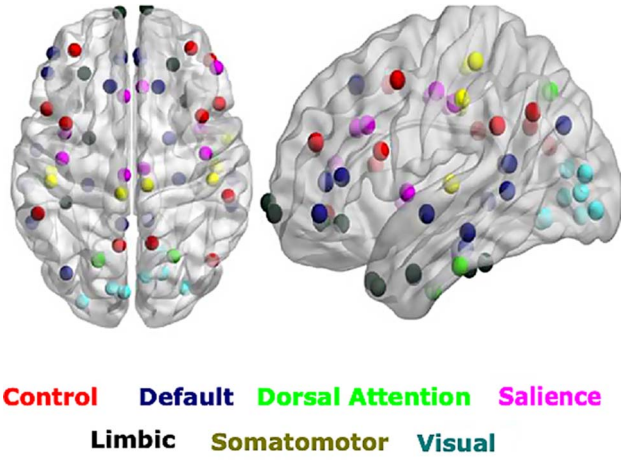

Figure 1. ROIs selected based on seven networks resting-state parcellation. The ROIs (circles) related 3 prominent brain networks are overlaid on the spatial distribution maps derived from group ICA of multiple resting-state networks of interest, that is, the DMN ROIs, the SN ROIs, and the control network or CEN.

The data driven approach consisted of characterization of age-associated functional connectivity differences and hub reorganization (see Supplementary Materials and Methods). Large-scale network hub selection and reorganization is plotted in Supplementary Figure 1. Based on the resemblance of the hub nodes (anchored in three neurocognitive networks) that was identified based on our analysis with frequently reported ROIs in the literature, we chose for our study inferior parietal lobule (IPL), PCC, and MOF as they constitute core part of DMN (Andrews-Hanna et al. 2010; Dixon et al. 2017) and consistently showed activation during mental rumination and self-related processing, mind wandering. The SN, which comprises the anterior insula and caudal, rostral ACC, is important for detection of salience events and switching between other large-scale networks (Menon and Uddin 2010; Uddin 2015). Bilateral rostral and caudal middle frontal gyrus (MFG) and superior parietal lobule (SPL) were selected as nodes of CEN. The core DMN regions selected in this work consistently showed anticorrelation with SNs (Fransson 2005; Uddin et al. 2009; Dixon et al. 2017).

For within network analysis, we used the extracted time series for each of the six ROIs within each respective network. For between-network analysis, we combined time series of the six ROIs using principal component analysis to create a single representative time series of each network (for further details, please see Supplementary Materials and Methods).

Directed Functional Connectivity

The main objective of the present study is to explore the directional changes and weighted causal outflow in the well-known triple resting-state networks across the lifespan and in the presence of exogenous drive from bilateral thalamus. In order to estimate directional functional connectivity in the time as well as frequency domain, we employed multivariate Granger causality analysis that is particularly suitable for our study (Reid et al. 2019). While we have specific hypothesis to be tested, we are not interested in understanding the underlying generative process or to settle a debate about mixed findings related to age-associated difference or no difference found in neurovascular coupling (Geerligs et al. 2015; Grinband et al. 2017). Dynamic causal modeling (DCM) would have been a more pertinent choice

Table 1 Coordinates of selected nodes of three resting-state networks according to Desikan–Killiany (DK) parcellation atlas

Networks	Brain regions	MNI coordinates (x, y, z)	
		Left (l)	Right (r)
Salience network	Insula	(−41, 13, −6)	(43, 12, −6)
	CACC	(−2, 21, 27)	(3, 21, 27)
	RACC	(−2, 39, 6)	(4, 38, 4)
Central executive network	RMFG	(−34, 53, 17)	(43, 45, 21)
	CMFG	(−45, 18, 46)	(43, 14, 43)
	SPL	(−25, −62, 63)	(17, −65, 59)
Default mode network	MOF	(−4, 44, −14)	(7, 45, −13)
	IPL	(−47, −70, 31)	(48, −67, 29)
	PCC	(−1, −18, 38)	(1, −16, 37)

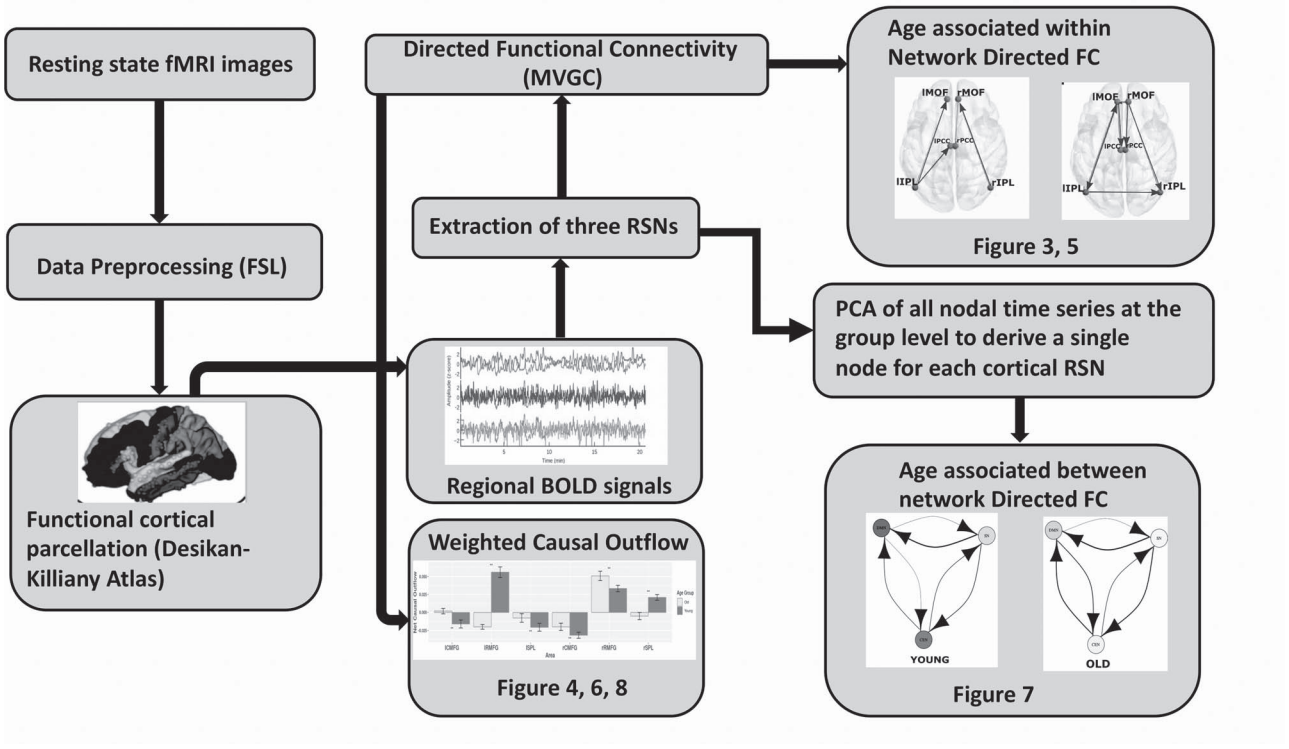

Figure 2. Flow chart describing major steps employed in our pipeline for estimation of directed functional connectivity and weighted causal outflow analysis using MVGC.

to investigate the latter research question. A flow chart describing major steps employed in our pipeline for estimation of directed functional connectivity and weighted causal outflow analysis using multivariate Granger causality (MVGC) is highlighted in the pipeline Figure 2. In the following section, we describe these steps in detail.

Multivariate Granger Causality Analysis

If we consider two variables X and Y that evolve over time, Y is said to G-cause X if the past values of Y contain information that helps predict the future of X over and above information in the past values of X alone (Granger 1969; Geweke 1982, 1984; Barnett and Seth 2014; Stramaglia et al. 2014; Barnett et al. 2018). This can be tested by constructing a univariate autoregression model of X and checking whether or not the lagged values of Y add any explanatory power to the model. However, neural signals from multiple brain regions are expected to show joint dependencies, thus necessitating the multivariate analysis. For instance, let $\mathbf{X_t}, \mathbf{Y_t}, \mathbf{Z_t}$ be the time series of 3 nodes in a network. If there are joint dependencies between $\mathbf{X_t}, \mathbf{Y_t}, \mathbf{Z_t}$ and if we calculate unconditional Granger causality between $\mathbf{X}$ and $\mathbf{Y}$, spurious causalities may occur due to the common dependency on $\mathbf{Z}$. Thus, to eliminate the possibility of spurious causalities between two time series, MVGC analysis was performed to assess the causal influence between nodes of the SN, CEN, and DMN based on the methods described in Barrett et al. (2010), Barnett and Seth (2014), and Seth et al. (2018). Group level analysis was performed with ROIs defined as variables, time points as observations, and subjects as trials. In MVGC, spurious systematic differences across brain regions in hemodynamic lag can potentially lead to spurious estimations of connectivity (Rangaprakash et al.

2018) and those connectivity and causality at the group level are eliminated by conditioning out the common dependencies (Seth et al. 2018). Thus, to test the G-causality from **Y** to **X**, one needs to consider the full and reduced regressions of the following form:

$$\mathbf{X}_t = \sum_{k=1}^{p} A_{xx,k}\,\mathbf{X}_{t-k} + \sum_{k=1}^{p} A_{xy,k}\,\mathbf{Y}_{t-k} + \sum_{k=1}^{p} A_{xz,k}\,\mathbf{Z}_{t-k} + \varepsilon_{x,t} \quad (1)$$

$$\mathbf{X}_t = \sum_{k=1}^{p} A'_{xx,k}\,\mathbf{X}_{t-k} + \sum_{k=1}^{p} A'_{xz,k}\,\mathbf{Z}_{t-k} + \varepsilon'_{x,t} \quad (2)$$

Here p is the model order, A is the regression coefficient, and ε the residuals. In full regression (1), the dependence of X on the past values of Y, given its own past values and the past values of Z is incorporated in the coefficients $A_{xy,k}$. If there is no conditional dependence of X on the past values of Y, this coefficient becomes zero. This leads to the reduced regression equation (2). Therefore, the null hypothesis of zero causality is:

$$H_0 : A_{xy.1} = A_{xy.2} = \cdots = A_{xy.p} = 0 \ \text{ vs.} H_1 : \text{at least one } A_{xy.k} \neq 0 \text{ for } k = 1, \cdots, p \quad (3)$$

The G-causality value quantifies the degree to which the full regression model is a better candidate compared with the reduced regression to model $\mathbf{X}_t$. An appropriate measure for the model comparison or prediction error in directional connectivity between selected pairs of nodes is the logarithm of the ratio of their likelihood values. The joint likelihood of the var model is $L = \left|\Sigma^{\frac{-(m-p)}{2}}\right|$ (where $|\Sigma|$ = the generalized variance of the model, m = total number of nodes, p = estimated model order). The conditional G-causality from Y to X in equations (1) and (2) is defined as:

$$F_{y\to x} = \ln\left|\frac{\Sigma'_{xx}}{\Sigma_{xx}}\right| \quad (4)$$

where $\mathrm{cov}(\varepsilon_{x,t}) = \Sigma_{xx}$, $\mathrm{cov}(\varepsilon'_{x,t}) = \Sigma'_{xx}$ are the error variances of the full model and reduced model, respectively. Although three time series were considered in the above example, in general, vector autoregressive (VAR) modeling is employed for each time t deals with a n-dimensional vector space with column vector U represents a multivariate time series signal. Therefore, a pth order VAR model can be represented using the similar notations as above in equations (1) and (2) as:

$$U_t = \sum_{k=1}^{p} A_k \quad U_{t-k} + \varepsilon_t \quad (5)$$

We employed the MVGC toolbox (Barnett and Seth (2014)) to perform the connectivity analysis. Joint likelihood L was calculated for each model order p up to the maximum model order. In practice, given empirical time series data, the model order p should be selected based on some theoretical criterion. The value of p should be sufficiently large to capture the predictive variation, but very large values of p are also not desirable, because they will induce over-fitting in the model. The order of the VAR model used for computation of the influence measure was selected using the Bayesian information criterion (BIC; Barnett and Seth (2014)). The model with lowest BIC was chosen. The choice of lowest BIC values resulted in a model order of $p = 2, 3$ in most cases while estimating within and between-network directed functional connectivity. Corresponding VAR model parameters, VAR model coefficients, and covariance matrices were estimated for the estimated model order. Using the reverse solution of the Yule Walker equations (Barnett and Seth 2014), the autocovariance sequences were calculated. For Granger causal estimation, VAR parameters were calculated for both the full and reduced regressions. Granger causality value was calculated using (4). Significance was tested using nonparametric analysis and F-tests as employed in Uddin et al. (2011) and Barnett and Seth (2014). Empirical null distributions of the influence of one node on another based on F-values and their differences were estimated nonparametrically using bootstrapping and surrogate analysis with null hypothesis of no causal interactions between the brain regions. Since multiple causalities were tested simultaneously, false discovery rate (FDR) correction was used to adjust for multiple hypotheses. The main strength of MVGC is that using the multiple equivalent representation of a VAR model by regression parameters, the autocovariance sequence, one is able to compute G-causality with the simultaneous estimation of full and reduced regression. This increases the power of statistical tests as well as model estimation accuracy.

Network Analysis

We estimated and quantified the following metrics to further characterize the networks in the young and elderly cohorts: (1) out-degree, number of causal outflow connections from a node in the network to any other node; (2) in-degree, number of causal in-flow connections to a node in the network from any other node; and (3) (out–in) degree, difference between out degree and in degree, a measure of the net causal outflow from a node. This permitted comparison with previously reported causal outflow measures in large-scale brain networks (Sridharan et al. 2008; Uddin et al. 2011).

We calculated the weighted net (Granger) causal flow. The main differences from previous work were that we employed here weighted net causal flow of a node, which was defined as the weighted (out–in) degree instead of what was previously employed and described above. This decision was made to account for the fact that unweighted estimates actually may lead to incorrect inferences about causal structure. Weighted out-degree of a node is the sum of the strength (i.e., Granger causal indices) of significant causal connections from the node to all the other nodes in the network. Likewise, weighted in-degree of a node is the sum of the strength of significant causal connections to that node from remaining nodes in the network. For example, weighted net causal outflow of node X, say Δ_x can be expressed using the following formula:

$$\Delta_x = (F_{x\to y} + F_{x\to z}) - (F_{y\to x} + F_{z\to x}) \quad (6)$$

provide all F values are significant. Nonsignificant F-values should be instead replaced by zero. Similarly, one can calculate Δ_y, Δ_z. Though F values are positive, weighted net causal values can be positive as well as negative. Positive Δ for a particular node implies higher causal influence of that node on the other nodes of the network, whereas negative Δ signifies that the particular node is more causally driven by other nodes of the network (in other words more inflow). These net causal outflow measures are used to characterize the hub of any causal flow network and redefine the role of hubs with age-associated alterations. In this definition, the node with the highest net causal outflow in a network is considered to be the hub of that particular network.

To compare the net flow of different nodes between young and old age groups, we generated 100 samples of Granger causality index matrices via nonparametric bootstrap sampling. For

the purpose of comparison, we constructed the distribution of weighted net causal outflow based on the significant causal connections ($P < 0.05$, FDR corrected for multiple comparisons). The distribution of weighted net causal outflow was calculated for different nodes within and between networks, and Wilcoxon signed rank tests were performed to test the significant differences in the net causal outflows for the different age groups.

Code Accessibility

All codes used for fMRI data analysis, causality estimation, and generation of manuscript figures are freely available from GitHub Cognitive Brain Dynamics Lab repository (URL below) and also upon reasonable request from the corresponding author, https://github.com/dynamicdip/CBDL_Granger_causal_AGING_fMRI.

Results

Age-Associated Within- and Between-Network Causal Connectivity Causal Connectivity Among Major Neurocognitive Networks

Within Network-Directed Functional Connectivity in Young Versus Elderly

We used MVGC analysis (Barnett and Seth 2014) to investigate causal interactions between the six network nodes in the three well studied neurocognitive networks. In the CEN, we extracted time series from six nodes (see Fig. 1), namely lRMFG, rRMFG, lCMFG, rCMFG, lSPL, and rSPL. The strength of the directed interaction from the rRMFG (driver node in a network) to the rCMFG (follower node in a network) was highest among all causal interactions for both the groups (Fig. 3A,D). There were no bidirectional interactions in the CEN. Interestingly, we did find rostro-caudal directed interactions in the CEN. Furthermore, there were substantial unidirectional drive from anterior regions of the CEN to the posterior regions along the anterior–posterior axis. We found significant directed functional connectivity ($P < 0.01$, FDR corrected) from the lRMFG to the lCMFG, and the lSPL for young individuals (restricted to a single hemisphere) (Fig. 3D). On the other hand, for the elderly group, significant directed functional connectivity was from the rRMFG to the lSPL (between two hemispheres) and rSPL (in addition to the rCMFG) (Fig. 3A). In contrast to DMN, a greater number of inter hemispheric connections were found in elderly individuals in the CEN (Fig. 3A).

To further investigate the network properties, we quantified weighted net causal outflow for the six nodes within CEN. The lRMFG and rRMFG (bilateral rostral areas in the Frontal Gyrus) acted as a causal outflow hub for young and elderly groups respectively. The majority of the identified causal outflows were significantly different for all the six nodes ($P < 0.01$). With the exception of lRMFG and rRMFG, all nodes had negative causal outflow (causal inflow) for young individuals (Fig. 4A). In contrast, in the elderly group, other than rRMFG, only lCMFG had small positive outflow. All the remaining nodes of the CEN had causal inflow. We have further estimated directed FC and weighted causal outflow for the CEN using BOLD signals of shorter duration (8 min 40 s resting-state data) and found qualitatively similar results confirming modality selective role of thalamus in mediating resting-state causal interactions (see Supplementary section and Supplementary Fig. 2 for more details).

Next we proceed with analysis of the SN which comprise of six nodes (see Fig. 2), namely lInsula, rInsula, lcACC, rcACC, lrACC, and rrACC. For within network analysis, quantitative comparison of MVGC analysis at the group level revealed a smaller number of significant directed causal influences compared with DMN and CEN. There was significant directed influence from lInsula to the lCACC, and the lRACC in young and elderly groups (Fig. 3B,E). Additionally, in the young group, significant directed influences were found from the rInsula to the rCACC and from the lRACC to the lInsula. One interesting find is that rInsula drives the rCACC in the young group but not in elderly group (Fig. 3E).

Weighted net causal outflow based on (out–in degree) analysis revealed lInsula as a major causal outflow hub in the SN for both age groups, but between group differences were also significant. In the elderly group, the causal outflow significantly reduced compared with young (old < young, $P < 0.01$, FDR corrected). Furthermore, rInsula had a small causal outflow in both groups, and the group differences were statistically significant ($P < 0.01$) and opposite of what is observed for the lInsula. The causal outflow from rInsula is significantly increased for the elderly group. lRACC had positive outflow for the young group and was significantly different for the elderly group (Fig. 4A,B). All the remaining nodes of ACC had negative outflow (causal inflow) for both groups. Causal outflows/inflows were significantly different ($P < 0.01$) for all the nodes.

We next applied MVGC analysis on the extracted time series for each of the six DMN nodes (see Fig. 1) for both young and elderly group to quantify the age effects in the dominant direction of influence ($P < 0.05$, FDR corrected). While in the younger group, MVGC analysis revealed significant directed causal connectivity from the lMOF (a driver as well as driven node) to the lIPL (bidirectional connectivity), lPCC (unidirectional) (follower nodes), and rMOF (a driver node) to the rIPL, rPCC, lMOF (interhemispheric-directed functional connectivity), and lIPL to rIPL (interhemispheric connectivity) as shown in Figure 3F, in elderly individuals, such bidirectional and interhemispheric causal connectivity was not present. Moreover, we see a reversal in the directed causal connectivity lIPL driving both lMOF and lPCC, and interhemispheric causal connectivity between lIPL to rIPL was completely absent (Fig. 3C), suggesting an age-associated decrease in causal drive within DMN nodes. This age-associated decrease in the causal drive within DMN nodes were also observed with resting-state BOLD signals with a shorter time duration and plotted in Supplementary Figure 3 (see Supplementary Materials and Methods).

Next, we estimated weighted net causal outflow or weighted (out–in) degree in both young and elderly group. Based on the 100 bootstrap samples, the distribution of weighted net causal outflow was calculated for each of the 6 nodes in DMN. For the young cohort, rMOF acted as a causal outflow hub among the nodes in DMN and was significantly different between the two groups (Mann–Whitney U test P value < 0.001), whereas rIPL acted as causal outflow hubhub for elderly group but acted as causal inflow hub for younger group (Fig. 4C,D). rPCC and lPCC both acted as causal inflow hubs receiving more drive from other nodes in the DMN for both young and elderly and were statistically significantly different in young group compared with old (Mann–Whitney test P value < 0.001). Interestingly, lPCC showed a reduction in causal inflow from young to old (young > old) while opposite was observed for the rPCC (old > young). Taken together, these results based on within network weighted causal flows (out-in degree) suggest an age-associated decrease in causal drive and suggests decline in within network DMN functional connectivity.

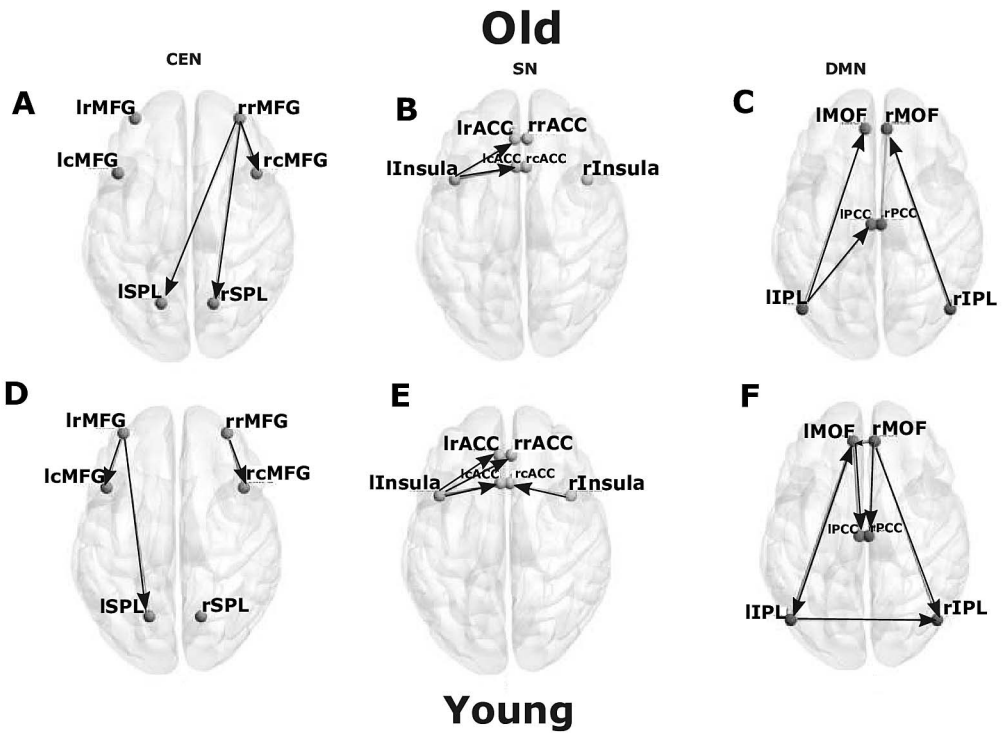

Figure 3. Directed functional connectivity between the nodes of three resting-state networks. Directed functional connectivity between (*A*) 6 key nodes of CEN, (*B*) 6 key nodes of SN, (*C*) 6 key nodes of DMN for elderly group. (*D*) 6 key nodes of CEN, (*E*) 6 key nodes of SN, (*F*) 6 key nodes of DMN for young group.

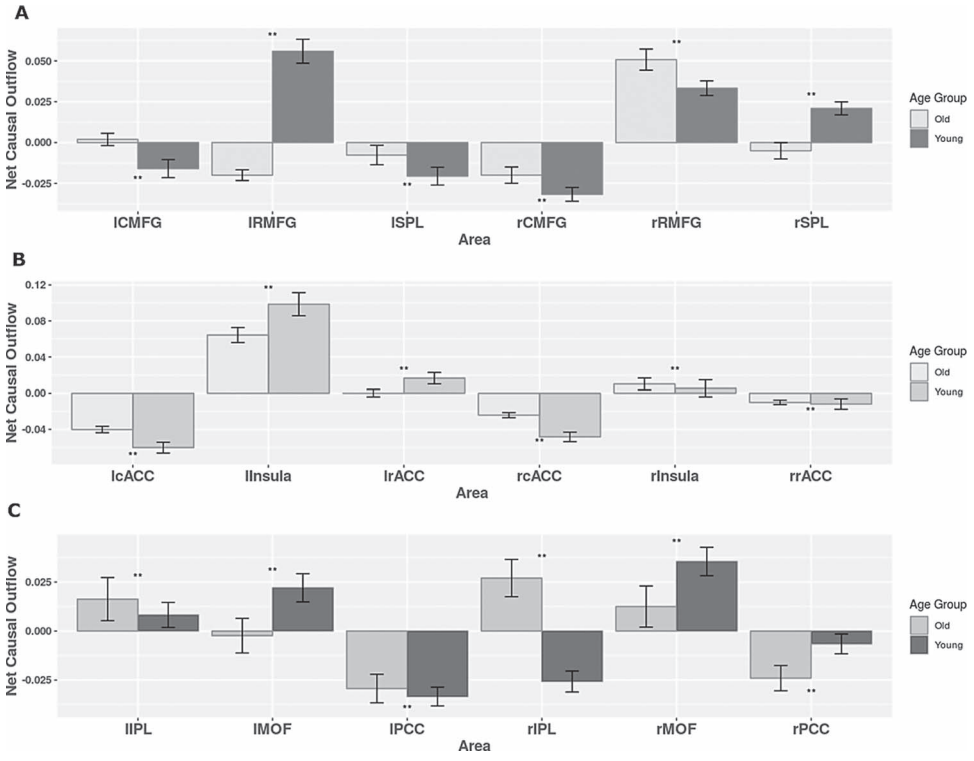

Figure 4. Weighted net causal outflow for within-network directed functional connectivity analysis. (*A*) Weighted net causal outflow in nodes of the central executive network. (*B*) Weighted net causal outflow in nodes of the salience network. (*C*) Weighted net causal outflow in nodes of default mode network. Weighted net causal outflows were significantly different in few nodes in each of the three RSN young and elderly group ($P < 0.05$ is indicated by "*" $P < 0.01$ is indicated by "**," no significant difference is indicated by "NS").

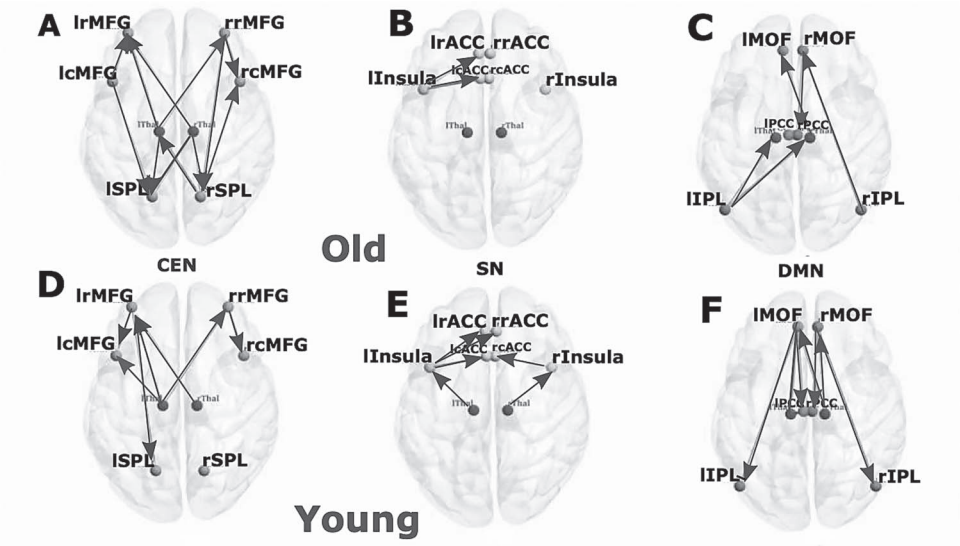

Figure 5. Directed functional connectivity between the nodes of three resting-state networks and the thalamus. (*A*) Directed functional connectivity between six key nodes of CEN, (*B*) six key nodes of SN, (*C*) 6 key nodes of DMN for elderly group in presence of thalamic nodes. (*D*) Directed functional connectivity between 6 key nodes of CEN, (*E*) 6 key nodes of SN, (*F*) 6 key nodes of DMN for elderly group in presence of thalamic nodes for young group in presence of thalamic nodes.

Reconfiguration of Within-Network Directed Functional Connectivity Associated with Age and Thalamocortical Interactions

In elderly group, all the connections except rRMFG-rlSPL remained significant ($P < 0.05$, FDR corrected) in the analysis including the thalamus. The connections between rRMFG–lSPL were mediated by the lThal. Some significant unidirectional causal connectivity was emerging from both the thalami, between lthal-lRMFG and rthal-lRMFG. In the CEN, we found frontal cortex was specifically driven by both left and the right thalamus in the left hemisphere. For both young and elderly groups, right and left thalamus were driving bilateral RMFG in the respective opposite hemispheres. Bilateral SPL was driven by rostral and caudal MFG in the elderly. Moreover, there were significant rostro-caudal interactions in the young as well as elderly group, but the direction of influence was reversed (Fig. 5*A*,*D*). For the young group, all the connections without thalamus were also found significant after inclusion of the thalamus (Fig. 5), which demonstrates that the overall patterns did not change by incorporating thalamo-cortical interactions. Rather, the evidence suggests that thalamic influence is absolutely critical to understand the variance of the prediction-errors for the estimation of directed functional connectivity in the triple resting networks. Additionally, the left thalamus exhibited directed functional connectivity among the following nodes of CEN: the lRMFG, the lCMFG, and the rRMFG (Fig. 5*D*). Right thalamus was the driver node and lRMFG was the follower node in the younger group.

Net Granger causal outflows were significantly changed after inclusion of thalamus for both the young and elderly groups. The effects of the thalamus were greater in the younger individual's weighted (out–in degree) net causal values (Fig. 6*A*). The left thalamus acted as a causal outflow hub for both the groups, as expected from the above results. However, the weighted causal outflow in the left thalamus was higher in the young group compared with the elderly group. We found significant group differences in weighted causal flow analysis for all the eight nodes ($P < 0.01$).

Among the three resting-state networks, the SN was least affected after inclusion of thalamus. No changes were found in causal structure after inclusion of thalamus in elderly individuals (Fig. 5*B*). In young individuals, significant causal connections were found from the lThal-lInsula connections ($P < 0.01$, FDR corrected) and from the rThal–rInsula connections ($P < 0.01$, FDR corrected) (Fig. 5*E*). No significant changes were found in the net causal outflow pattern in both the groups. Left thalamus exhibited positive outflow, higher in the case of older individuals ($P < 0.05$). Right thalamus received marginally small negative outflow (inflow) for both groups (Fig. 6*A*,*B*).

Next, we studied causal interactions between thalamus and the DMN. We observed significant reconfiguration in the directed functional connectivity pattern found in the elderly individuals. On performing MVGC analysis on DMN after addition of thalami, some of the earlier significant causal connections disappeared while some thalamo-cortical causal connections emerged as important connections for both the age groups (Fig. 5*C*,*F*). The reversal of unidirectional connectivity between rIPL–rMOF follows a posterior–anterior gradient and anterior–posterior gradient, as seen previously in the connections rMOF–rIPL. Posterior–anterior directional connectivity continued to be the strongest in elderly group without taking into account thalamic interactions (Fig. 5*C*). Other than that, MVGC revealed significant causal connections from the rMOF to the rPCC, from the rThal to the lIPl, from the lIPL to the rThal, from the rThal to the lMOF for elderly people (Fig. 5*C*). In the presence of thalamo-cortical causal interaction, directed functional connectivity between the left hemispheric nodes were largely absent in elderly. For the young group, the effect of the thalamus was more pronounced compared with the elderly group (young > old) (Fig. 5*F*). Instead of the connection from the lMOF to the lPCC, the connection from the lThal to the lPCC emerged as the strongest connection after the inclusion

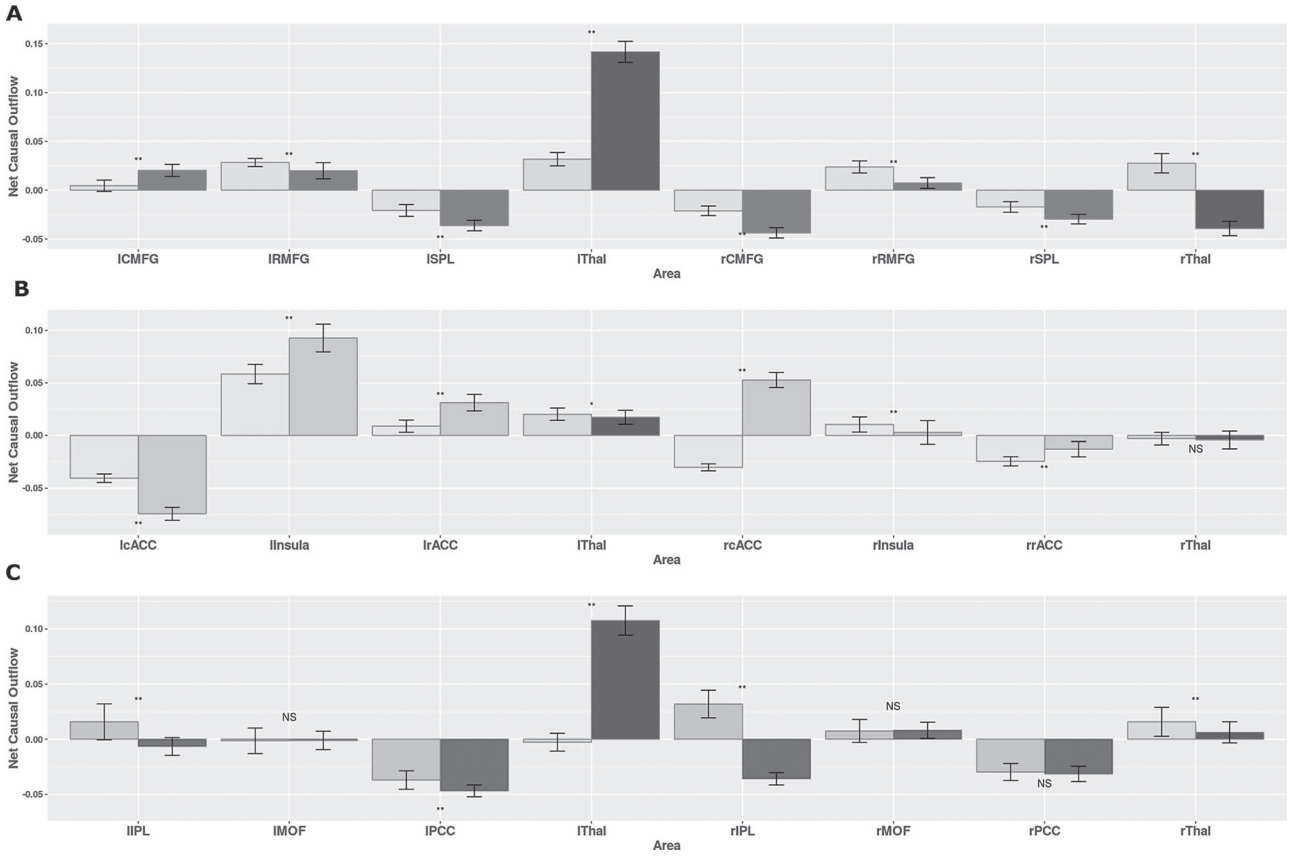

Figure 6. Weighted net causal outflow for within-network directed functional connectivity analysis. (*A*) Weighted net causal outflow in nodes of the central executive network and two thalamic regions (left, right). (*B*) Weighted net causal outflow in nodes of the salience network and two thalamic regions (left, right). (*C*) Weighted net causal outflow for default mode network and two thalamic regions (left, right). Weighted net causal outflows were significantly different in nodes in each of the three RSNs for young and elderly group ($P < 0.05$ is indicated by "*," $P < 0.01$ is indicated by "**," no significant difference is indicated by "NS").

of the thalami (though the lMFCOF to the lPCC connection also remained significant). In addition, other significant connections were from the lMOF to the lIPL, from the lThal to the lMOF, from the lThal to rThal, from the lThal to the rPCC, from the rThal to the lMFC, from the rThal to the rMFC, from the rMFC to the rPCC, and from the rMFC to the rIPC (Fig. 5F), suggesting substantial effects of thalamus in reorganizing within-network causal drive this network, and also revealing the effect is the strongest in the younger group compared with the elderly.

Net Granger causal outflows were significantly changed after accounting for cortico-thalamic causal interactions, in particular, for the young group. Among the two thalami, the left thalamus emerged as a causal outflow hub for the young group, exhibiting substantial drive to the cortical nodes in the DMN Patterns in the weighted net causal outflows remained unchanged in elderly group (Fig. 6C). Right hemispheric IPL continued to be causal outflow hub for elderly group were significantly different ($P < 0.01$, FDR corrected) from the young group, even after accounting for thalamo-cortical interactions. Causal outflows were significantly different in both groups ($P < 0.01$). Overall, we found stronger weighted causal outflow and increase causal drive from the thalamus among key nodes (left and right IPL, left and right PCC) of the DMN network associated with aging.

Reconfiguration of Between-Network Directed Functional Connectivity Associated with Age and Thalamocortical Interactions

Next, we asked in what specific way the between-network interactions in the three neurocognitive networks are reconfigured by age and cortico-thalamic interactions. To address this systematically, we employed principal component analysis (PCA) to combine the time series from each of the resting-state networks (CEN, SN, and DMN). We took the first principal component of all nodal time series of a network that resulted in maximum explained variance of the signal. Subsequently, we performed MVGC among three nodes derived from the first principal component of each cortical RSNs at the group level. Each of these three principal nodes for all subjects combined in both young and elderly groups were representative nodes of CEN, SN, and DMN respectively.

In between-network analysis, SN exhibited stronger causal influence on both DMN and CEN (SN > DMN and SN > CEN) in both young and old groups (Fig. 7A,B). Directed functional connectivity and causal strengths were significantly stronger in old groups compared with young ($P < 0.01$, FDR corrected). Furthermore, with age, both CEN and SN exerted stronger directed functional connectivity with DMN ($P < 0.01$, FDR corrected) and internetwork connectivity between SN and CEN got significantly

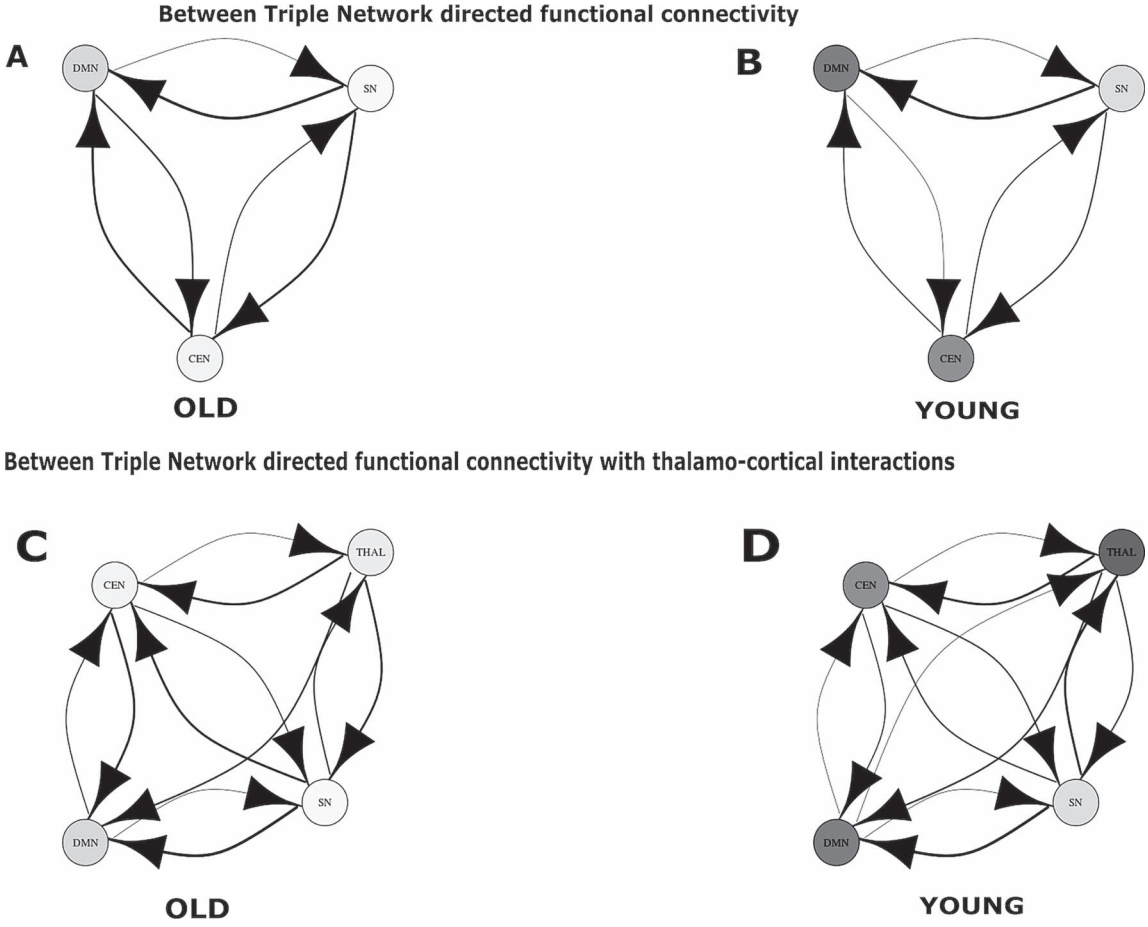

Figure 7. Directed functional connectivity between three resting-state networks in absence and presence of the thalamus. (*A*) Directed functional connectivity between three nodes representing three RSN, SN, DMN, CEN for old population. (*B*) Results for directed functional connectivity between three nodes representing three RSN for young population. (*C*) Directed functional connectivity between three nodes representing three RSN and fourth node representing the thalamus for old population. (*D*) Directed functional connectivity between three nodes representing three RSN and fourth node representing the thalamus for young population.

stronger with age ($P < 0.01$, FDR corrected). With thalamocortical interaction (Fig. 7C,D), there was presence of bidirectional interactions between thalamus and SN (in the young group) and in turn SN mediated directed functional connectivity with both DMN and CEN. As in the absence of thalamocortical interactions DMN had greater directed functional connectivity with SN compared with CEN in the young group. In the older group, we found that thalamus is the key driver which exhibit greater (old > young) directed functional connectivity with SN and in turn, SN exhibits stronger directed functional connectivity with CEN and DMN both. Taken together these results confirms our hypothesis of overall stronger directed functional connectivity strength in the old group compared with the young group, suggesting an age-associated increase in between-network directed functional connectivity mediated by SN, however, when thalamocortical interactions are taken into consideration then thalamus emerges as key integrating hub driving causally neurocognitive networks CEN, DMN via SN, which subserve the role of a key mediator (connector hub) and facilitate increased internetwork interactions.

Next, we estimated the weighted net Granger causal outflow among three neurocognitive networks. We found among the three cortical RSNs, the SN was a causal outflow hub driving both DMN and CEN. Network causal outflows (in–out degree) were statistically significantly different between young and elderly groups ($P < 0.01$, FDR corrected) (Fig. 8A). Further, we repeated between-network analysis, with the second principal component of all nodal time series of a network. No significant directed functional connectivity was found, confirming the fact that the first principal component sufficiently explained all the variabilities present in the time series of the three networks.

The weighted net causal outflows were significantly affected after taking into account thalamocortical interactions. We find evidence for the thalamus acting as a causal outflow hub (old > young) for the elderly group (Fig. 8A). Interestingly, SN and CEN dynamics were completely antagonistic with each other based on weighted causal outflow in the presence of cortico-thalamic interactions. DMN also exhibited greater causal inflow with respect to age. While SN received highest weighted causal outflow for young group (young > old, $P < 0.01$, FDR corrected) CEN received highest causal inflow for elderly group (old > young) (Fig. 8B). Unlike the within-network results, in between-network analysis, causal outflows were greater in the elderly group with or without accounting for thalamocortical causal interactions confirming our hypothesis that there is an age-associated increase in internetwork causality and thalamus

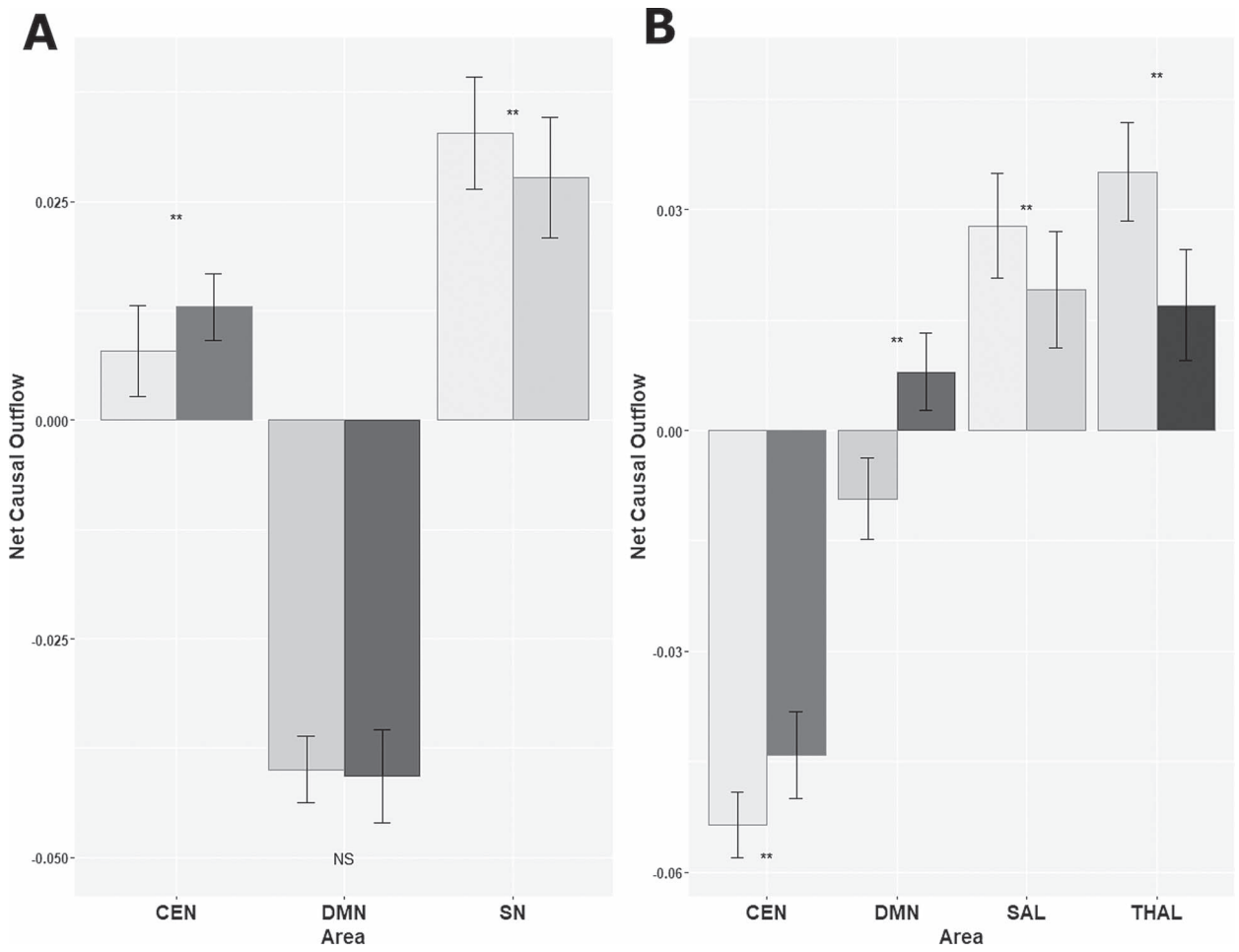

Figure 8. Weighted net causal outflow for between-network directed functional connectivity analysis. (*A*) Weighted net causal outflow in three RSN. (*B*) Weighted net causal outflow in three RSN and the thalamus. Weighted net causal outflows were significantly different in few nodes in each of the three RSN young and elderly group ($P < 0.01$ is indicated by "**," no significant difference is indicated by "NS").

plays the key role of an integrative hub in organizing causal information outflow among major neurocognitive networks. Analysis with resting-state BOLD signal of shorter duration confirmed these results were not influenced by the long scan duration (Supplementary Figs 4 and 5, see Supplementary Materials and Methods for details).

Overall, thalamo-cortical interactions alter the directed functional connectivity patterns and causality between the triple networks. However, the thalamus also received feedback causal influences and driven by both the SN and CEN particularly in the young group, and in the elderly group, DMN was driven strongly by the influence of SN which was driven by thalamus. Hence, the weighted net causal outflows for the elderly group were affected accounting for substantial thalamo-cortical interactions. However, this is hardly surprising given that left thalamus in particular emerged as an important causal hub node in mediation of crucial thalamo-cortical interactions with respect to age. Taken together, within-network thalamic drive progressively weakens with age, and stronger directed functional connectivity was found in the young group between thalamo-cortical connections. On the contrary, in the elderly group, between-network directed functional connectivity was far less dissimilar accounting for thalamo-cortical interactions.

Replication Analysis

We identified a group of 24 young and 25 elderly participants from the publicly available Cambridge Aging Neuroscience dataset (https://camcan-archive.mrc-cbu.cam.ac.uk//dataaccess/) in the age range of 18–80 years who did not differ in mean age, gender distribution from Berlin dataset (see methods). Using this new dataset for independent validation, we conducted identical directed functional connectivity and weighted causal outflow analyses for each of the 3-core neurocognitive resting-state networks of interest. In the replication analysis, the 6 nodes for CEN included bilateral caudal MFG (rCMFG, lCMFG), rostral MFG (rRMFG, lRMFG) and superior parietal lobule (rSPL, lSPL).

We found several significant overlaps in the within-network causality results between the connections between rRMFG–lSPL and lRMFG–rSPL and these connections were mediated by both the lThal and rThal, respectively. Some significant unidirectional causal connectivity was emerging from both the thalami, between lthal–lRMFG and rthal–lRMFG ($P < 0.05$, FDR corrected). In the CEN, we found frontal cortex was specifically driven by both left and the right thalamus in the left hemisphere as was observed in the original data. For both young and elderly groups, right and left thalamus were driving bilateral RMFG in the respective opposite hemispheres. Bilateral SPL was

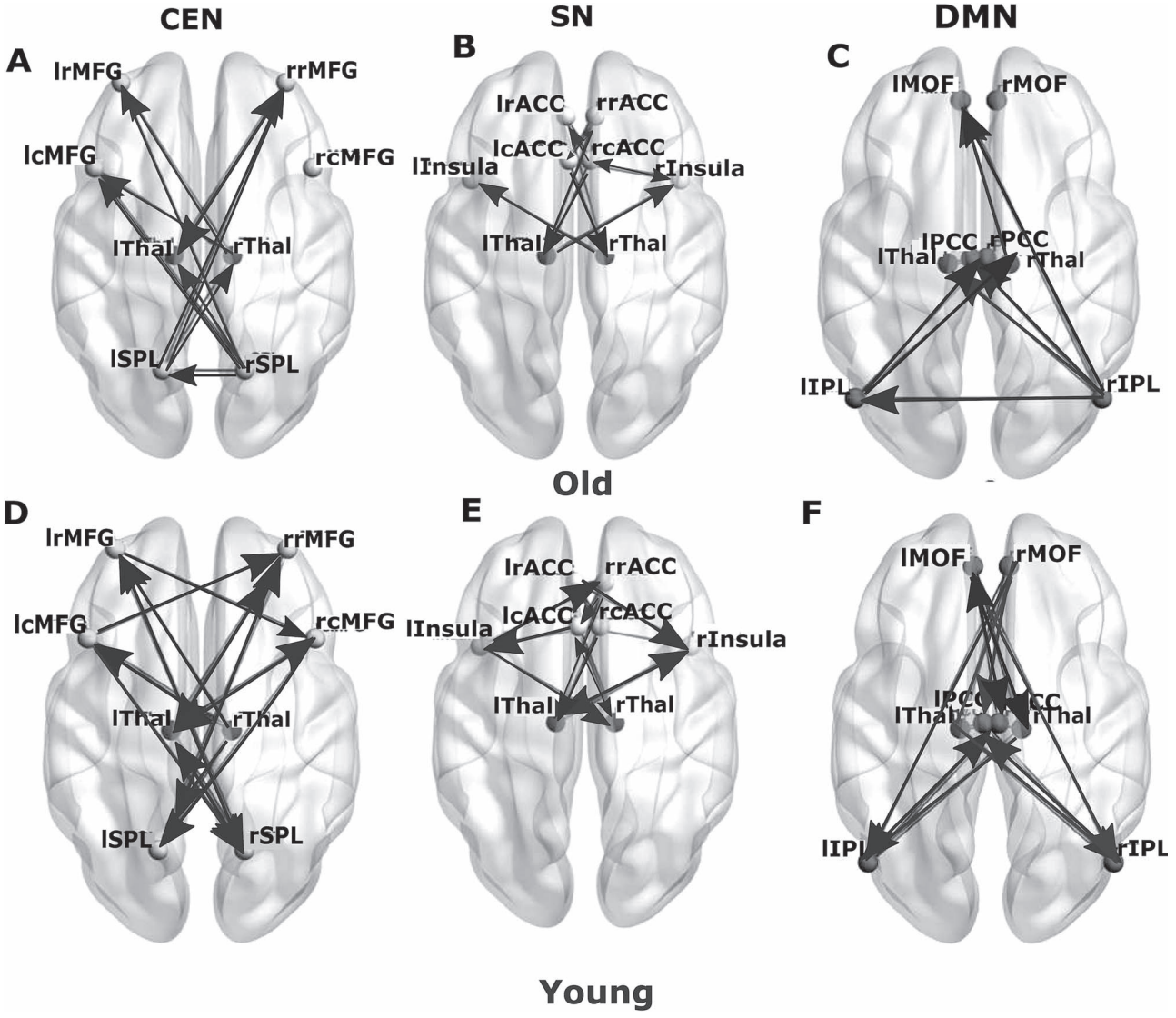

Figure 9. Directed functional connectivity between the nodes of three resting-state networks and the thalamus in the replication analysis. Directed functional connectivity between (*A*) key nodes of CEN, (*B*) key nodes of SN, (*C*) key nodes of DMN for elderly group in presence of thalamic nodes (blue). (*D*) Directed functional connectivity between key nodes of CEN, (*E*) key nodes of SN, (*F*) key nodes of DMN for young group in presence of thalamic nodes.

driven by rostral and caudal MFG in the elderly. There were some differences as well. While there were significant rostrocaudal interactions as in the original data, but this time it was only present for the elderly and not for the young. There was interhemispheric-directed functional connectivity between bilateral parietal lobule which was absent from the Berlin data. In replication analysis, we discovered in the elderly group rSPL (a driver node) was having significant directed functional connectivity ($P < 0.05$, FDR corrected) with lSPL (a follower node). Significant connections ($P < 0.05$, FDR corrected) emerged from left and right thalami both in the young and old groups. However, the number of causal connections between thalamus and CEN nodes were greater in the younger cohort (Fig. 9*A*,*D*).

Bilateral rostral anterior cingulate (rrACC, lrACC), caudal anterior cingulate (rcACC, lcACC), and insula (rIns, lIns) were defined as the nodes of the SN. We observed directed functional connectivity between bilateral insula (driver) and caudal ACC (driven by Insula). We also found a difference while bilateral insula was driven by thalamus in the young group in the original data, this connection was absent for the old group. In the replication analysis, this connection did not disappear in the old group (Fig. 9*B*,*E*). In both datasets, the number of connections decreases significantly in the old group compared with young.

In the DMN, the nodes selected were bilateral medial orbitofrontal (lMOF, rMOF), IPL (lIPL, rIPL), and PCC (lPCC, rPCC). In the younger group, MVGC revealed extensive causal connections between all the DMN nodes (Fig. 9*F*), which was missing in the older group. In both data, we found there is significant overlap between anterior–posterior interactions and the connections also exhibited hemispheric asymmetry in the older group.

The younger cohort exhibited a greater number of causal interactions than the older group (Fig. 9*C*,*F*), suggesting an age-related decrease in within DMN causal drive. Significant causal

connections ($P < 0.05$, FDR corrected) emerged from left and right thalami both in the young and old groups. However, the number of causal connections between thalamus and DMN nodes was greater in the younger cohort (Fig. 9F). We also found similarity in directed functional connectivity between bilateral IPL and bilateral MOF and missing lIPL–lMOF connections in original and replication analysis. In the replication data, we also discovered reversal of anterior–posterior directed connections between MOF and IPL associated with age as was found in the original data. There was a difference, rIPL was driven by rMOF in the original data and this directional functional connectivity reversed in older group. In the replication data, rIPL was driven by lMOF and not by rMOF and the directionality was similarly reversed in the older group as was found in the original data.

To represent the information of all the nodes in a particular network for a between-network analysis, the time series of all the nodes in each of the resting-state network were combined by employing a PCA (see Methods). All causal connections were found significant.

Between-network directed functional connectivity showed significant overlap between SN, CEN, DMN connections in the young and old group in both data. In the young group, we discovered that SN (a driver network) exhibits strongest directional functional connectivity with both DMN (a follower network) and CEN (a follower network). Also, CEN drives DMN network causally and exhibits directed functional connectivity. In both replication data as well as original data, SN emerged as the key driver network exhibiting stronger directional functional connectivity with DMN and CEN associated with age. The number of directed functional connectivity as well strength increases with age which is an overlapping finding for both original and replication data (stronger between-network directed functional connectivity and increased internetwork causal outflow in neurocognitive networks with age; Fig. 10A,B). Finally, thalamo-cortical interactions did not necessarily alter any of the directed functional connectivity patterns between the neurocognitive networks; however, displayed directed connections only between CEN and thalamus in the older cohort (Fig. 10C). This was the main difference with original analysis, where we discovered other connections such as thalamus–SN, DMN–thalamus, and others. On the other hand, for both original and replication data in the young group, we found presence of overwhelmingly large number of bidirectional functional connectivity of neurocognitive resting-state networks with thalamus compared with elderly (Fig. 10D).

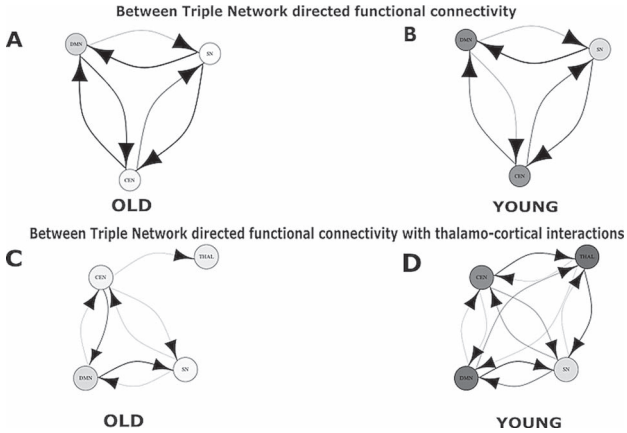

Figure 10. Directed functional connectivity between three resting-state networks in absence and presence of the thalamus for the replication analysis. (*A*) Directed functional connectivity between three nodes representing three RSN, SN, DMN, CEN for old population. (*B*) Results for directed functional connectivity between three nodes representing three RSN for young population. (*C*) Directed functional connectivity between three nodes representing three RSN and fourth node representing the thalamus for old population. (*D*) Directed functional connectivity between three nodes representing three RSN and fourth node representing the thalamus for young population.

Discussion

In the present study, we employ MVGC and weighted network causal outflow analysis to probe within- and between-network causal relationships among three key intrinsic resting-state brain networks with the hope of facilitating more biologically meaningful interpretations of brain signatures of healthy aging by taking into consideration the role of the thalamus as both a modality selective and an integrating hub. Based on our results, the thalamus exhibits both modality specific as well as integrator role in organizing causal information flow among large-scale neurocognitive networks. Based on within-network analysis, we have found that the thalamus acts in a modality selective manner by causally driving both CEN, DMN but less influencing SN. We also found that with age within-network causality diminishes perhaps suggesting weaker functional connections between the thalamus and those networks. However, there is a role reversal when it comes to mediating causal flow for the internetwork interactions. Here, we found thalamus emerges as a key integrative hub by strongly driving SN and subsequently, SN mediates causal information flow between DMN, CEN possibly maintaining hierarchy of information flow. Finally, we establish that the between-network causal drive increases with age (old > young) and mediated by both thalamus and SN, establishing the enhanced role of SN with age and dual role of the thalamus as a network driver.

Every cortical region receives feedforward projections from the thalamus and in turn sends outputs to one or multiple thalamic nuclei (McFarland and Haber 2002; Obeso et al. 2008). Thalamo-cortical projections relay nearly all incoming information to the cortex as well as mediate corticocortical communication (Sherman and Guillery 2002). Thus, deeper insight into brain functional characterization requires knowledge of the organization and properties of thalamo-cortical interactions. A recent study by Hwang et al. (2017) showed the thalamus as an integrative hub for functional networks. A handful of studies also observed disrupted thalamic resting-state functional networks in brain injury and schizophrenia (Tang et al. 2011; Wang et al. 2015). Also, it has been widely reported that thalamic volume significantly decreases with aging (Walhovd et al. 2005; Cherubini et al. 2009; Zheng et al. 2018). Goldstone et al. (2018) further investigated the association of thalamic functional connectivity with sensory and motor areas and relationship with behavioral performance of elderly individuals. However, there is a knowledge gap in terms of how thalamo-cortical interactions sculpt causal drive and how they reconfigure directed functional connectivity in major neurocognitive networks with aging. This knowledge-gap is surprising given that lifespan-associated behavioral performance and flexibility in principle is governed by large-scale functional brain network reorganization and whole brain dynamics at fast and slow time scales (Naik et al. 2017; King et al. 2018; Sahoo et al. 2020).

Previous evidence suggests that there is substantial subcortical–cortical causal interactions during maturation and

development (Menon and Uddin 2010; Uddin et al. 2011). Hence, focusing primarily on cortical networks and nodes in these analyses paints an incomplete understanding. Overall, we found significant dynamic reconfiguration of between- and within-network directed functional connectivity and weighted causality significantly alters with aging and in particular thalamo-cortical interactions are taken into account. After inclusion of the thalamus in the between-network analysis, we observed that the thalamus acts as a causal outflow hub, driving all three network nodes in both age groups. In contrast, in within-network analysis, the influence of the thalamus in reorganizing within-network causality is much more prominent in the younger age group compared with the older group. In the DMN, the left thalamus comes out as a causal outflow hub for the young group, while patterns in the net causal outflows were unchanged in the older group compared with what was observed in the absence of thalamo-cortical interactions. While considering thalamo-cortical interactions, within-network analysis in the CEN revealed that the left thalamus acts as a causal outflow hub for both the groups; however, the causal outflow strength was significantly greater in the younger compared with the older group. Finally, we also demonstrate how thalamo-cortical interactions play a crucial role in mediating within-network interactions among the specific neurocognitive networks in a modality selective fashion and the effects are particularly stronger in the younger group compared with elderly. Taken together this further suggests an age-associated thalamo-cortical decline in maintenance of within-network causality.

The question of segregated and integrated brain dynamics is fundamental and pertinent with regards to alteration and reconfiguration of brain network dynamics with aging. Hence, we focused on the decreased causal segregation of brain networks (i.e., increased internetwork directed functional connectivity), two features which can be considered a hallmark of the aging process. According to the dedifferentiation hypothesis of cognitive aging, age-related impairments in cognitive function arise from reduced distinctiveness of neural representations (Li et al. 2001). Historically, the concept of dedifferentiation was introduced by Baltes and colleagues (1980) to account for age-related increases in the correlation between levels of performance on different cognitive tasks. At the neural level, numerous brain-imaging studies have shown that the aging brain adapts by exhibiting more global activation compared with younger individuals while performing a cognitive/motor task (Cabeza 2002; Reuter-Lorenz 2002; Serrien et al. 2007; Seidler et al. 2010). In line with these finding, at the network level, several studies have found a decrease in within-network functional connectivity and an increase in between-network functional connectivity in RSNs with aging (Andrews-Hanna et al. 2007; Ferreira and Busatto 2013; Betzel et al. 2014; Geerligs et al. 2015; Ferreira et al. 2016; Ng et al. 2016). More specifically, younger individuals display increase in both the number and the strength of weighted causal within the nodes of DMN, CEN, and SN and the causal outflow strength increases compared with elderly (young > old) when thalamic interactions are further taken into account. At the between-network level, we find that causal strengths are significantly higher in the older individuals compared with the young, thus further substantiating the dedifferentiation hypothesis. Moreover, the present study also uncovers several novel observations. We observed the reversal of direction of causal connections in DMN between rMOF and rIPL with aging (change in directionality along anterior–posterior gradient), age-associated changes in the causal outflow in key nodes of DMN and CEN networks, and reconfiguration of weighted causal outflow hubs. This is in line with shifting hubs and default executive coupling hypothesis associated with healthy aging process (Naik et al. 2017; Spreng and Turner 2019). For future studies, it would be very interesting to see, by employing a similar methodology on a larger sample size including various stages of the adult lifespan, whether a clear trend emerges in directed functional connectivity patterns.

The role of the SN in mediating switching between DMN and CEN is well established (Sridharan et al. 2008; Menon and Uddin 2010; Goulden et al. 2014). In agreement with previous observations, we find the SN exerts strong causal influence on both DMN and CEN in both age groups. In between-network analysis, the SN is found to act as a causal outflow hub among the three RSNs. Interestingly, the causal influence of SN on both DMN and CEN increases with aging. An increase in the between-network causality in the older group emerges as a general trend in our analysis. This is a counterintuitive result as within network analysis actually revealed significant evidence for thalamic decline with age. However, it seems higher neurocognitive networks such as SN, CEN, DMN establish stronger between-network directed connections with the thalamus in the old group. Our study also reveals the salience network's role as a mediator of switching between DMN and CEN and establishes greater between-network directional connectivity in elderly compared with young (old > young). This finding is in line with the extant literature (Menon and Uddin 2010; Uddin et al. 2011; Bonnelle et al. 2012) and also provides confirmatory evidence of the pivotal role played by the SN for flexible switching as one of the major causal outflow hub. Among the 3 resting-state networks, the SN remains least affected after inclusion of the thalamus. We did not find substantial reconfiguration in SN with thalamo-cortical interactions in elderly individuals. Also, the reconfigurations of this network were minimal in the young group. The net causal outflow pattern also did not change after taking thalamo-cortical interactions into account for both the groups. This could be related to the underlying decline in cortico-thalamic connectivity with aging. These findings are in concurrence with the observations made by the previous studies (Cao et al. 2014; Wang et al. 2015; Sakaki et al. 2016; Xiao et al. 2018) that in contrast to the DMN and CEN, within-network connectivity is preserved or increased in SN with aging. Our result suggests that this preservation of causal connectivity patterns within SN may be crucial for aging and could be driven by thalamus.

We performed a replication analysis with an independent dataset controlling for age, gender, and some of the major findings with the original dataset were largely replicated. In within-network analysis, we observed greater number of causal connections and higher strengths in the younger group compared with older individuals are consistent with our findings with the original dataset. The effect of thalamo-cortical interactions was also revealed within-network directed functional connectivity diminishes in older individuals confirming our original hypothesis. Notably, we also found some specific differences between original and replication analysis. These differences may be attributed to site variability, sample size, individual variability in the samples and data acquisition parameters. For example, an obvious difference is the duration of resting-state scan and acquisition. They are certainly not identical in the 2 datasets (22 min for the Berlin data and 8 min 40 s for the CAM-CAN replication cohort). This observation prompted us to carry

out further analysis with BOLD resting data of shorter durations. We found qualitatively complete agreement with reported directed functional connectivity and weighted causal outflow results and age-associated alterations using shortened datasets (Supplementary Materials).

We acknowledge several limitations of our study that should be addressed in future work. First, the thalamus is a heterogenous structure composed of several nuclei, each of which sends distinct afferent inputs to cortical regions as well as being driven by cortical outputs. Thus, probing the influence of different nuclei of thalamus on reorganization of within- and between-network causality of different RSNs would help to better describe the complex neurophysiological processes taking place in the brain with aging. Theses analyses will require higher resolution fMRI data acquisition. Subsequently, analysis presented here could be extended to other subcortical regions to understand how cortical–subcortical connectivity impacts the cognitive performance and flexibility across age. Second, the hierarchical causal architecture among neurocognitive networks is an ongoing debate that can be resolved in the future using a DCM approach. Future studies using diffusion-weighted imaging can delimit the model space for optimizing maximum-likelihoods associated with specific directional functional connectivity. Finally, we acknowledge that the sample size in both groups are small, and it would be better to carry out analysis on larger lifespan cohort consist of data representing various stages of adult lifespan to gain insight onto the age-associated trends in causal outflow patterns.

In conclusion, the results of the present study demonstrate that directed functional connectivity and weighted causal analysis can provide critical insights regarding within- and between-network information flow across the lifespan over and above insights already provided by existing functional connectivity studies. This study firmly establishes that the bilateral thalamus presents itself in a dual position carrying out modality specific as well as an integrative hub role in driving causal information flow among prominent neurocognitive networks associated with healthy aging. This conclusion encourages future research to explore the influences exerted by subcortical structures on cortical networks and their cognitive and clinical implications.

Supplementary Material

Supplementary material is available at *Cerebral Cortex* online.

Funding

This study was supported by NBRC Core funds, Ramalingaswami Fellowships (Department of Biotechnology, Government of India) to D.R. (BT/RLF/Re-entry/07/2014). D.R. was also supported by SR/CSRI/21/2016 extramural grant from the Department of Science and Technology (DST) Ministry of Science and Technology, Government of India. A.B. and D.R. are also supported by BT/MED-III/NBRC/Flagship/Program/2019. L.U. is supported by R01 MH107549 grant from National Institute of Mental Health (NIMH) USA.

Replication data used in this study were generously provided as a public resource and repository by the Cambridge Centre for Ageing and Neuroscience (CamCAN). CamCAN funding was provided by the UK Biotechnology and Biological Sciences Research Council (grant number BB/H008217/1), together with support from the UK Medical Research Council and University of Cambridge, UK.

Notes

Conflict of Interest: None declared.

References

Abi-Dargham A, Horga G. 2016. The search for imaging biomarkers in psychiatric disorders. *Nat Med*. 22(11):1248–1255. doi: 10.1038/nm.4190.

Andrews-Hanna JR, Reidler JS, Sepulcre J, Poulin R, Buckner RL. 2010. Functional-anatomic fractionation of the Brain's default network. *Neuron*. 65(4):550–562. doi: 10.1016/j.neuron.2010.02.005.

Andrews-Hanna JR, Snyder AZ, Vincent JL, Lustig C, Head D, Raichle ME, Buckner RL. 2007. Disruption of large-scale brain systems in advanced aging. *Neuron*. 56(5):924–935. doi: 10.1016/j.neuron.2007.10.038.

Baltes PB, Cornelius S, Spiro A, Nesselroade JR, Willis S. 1980. Integration versus differentiation of fluid/crystallized intelligence in old age. *Dev Psychol*. 16(6):625–635. doi: 10.1037/0012-1649.16.6.625.

Barrett AB, Barnett L, Seth AK. 2010. Multivariate Granger causality and generalized variance. *Phys Rev E Stat Nonlinear Soft Matter Phys*. 81(4):041907-1-041907-14.

Barnett L, Seth AK. 2014. The MVGC multivariate Granger causality toolbox: a new approach to Granger-causal inference. *J Neurosci Methods*. 223:50–68.

Barnett L, Barrett AB, Seth AK. 2018. Misunderstandings regarding the application of Granger causality in neuroscience. *Proc Natl Acad Sci USA*. 201714497.

Beckmann CF, Smith SM. 2004. Probabilistic independent component analysis for functional magnetic resonance imaging. *IEEE Trans Med Imaging*. 23(2):137–152. doi: 10.1109/TMI.2003.822821.

Betzel RF, Byrge L, He Y, Goñi J, Zuo XN, Sporns O. 2014. Changes in structural and functional connectivity among resting-state networks across the human lifespan. *Neuroimage*. 102(P2):345–357. doi: 10.1016/j.neuroimage.2014.07.067.

Bonnelle V, Ham TE, Leech R, Kinnunen KM, Mehta MA, Greenwood RJ, Sharp DJ. 2012. Salience network integrity predicts default mode network function after traumatic brain injury. *Proc Natl Acad Sci*. 109(12):4690–4695. doi: 10.1073/pnas.1113455109.

Bressler SL, Menon V. 2010. Large-scale brain networks in cognition: emerging methods and principles. *Trends Cogn Sci*. 14:277–290. doi: 10.1016/j.tics.2010.04.004.

Buckner RL, Andrews-Hanna JR, Schacter DL. 2008. The brain's default network: anatomy, function, and relevance to disease. *Ann N Y Acad Sci*. 1124:1–38. doi: 10.1196/annals.1440.011.

Buckner RL, Krienen FM, Castellanos A, Diaz JC, Yeo BTT. 2011. The organization of the human cerebellum estimated by intrinsic functional connectivity. *J Neurophysiol*. 106(5):2322–2345. doi: 10.1152/jn.00339.2011.

Cabeza R. 2002. Hemispheric asymmetry reduction in older adults: the HAROLD model. *Psychol Aging*. 17(1):85–100. doi: 10.1037/0882-7974.17.1.85.

Cao W, Luo C, Zhu B, Zhang D, Dong L, Gong J, Gong D, He H, Shipeng T, Yin W *et al*. 2014. Resting-state functional connectivity in anterior cingulate cortex in normal aging. *Front Aging Neurosci*. 6:280. doi: 10.3389/fnagi.2014.00280.

Cherubini A, Péran P, Caltagirone C, Sabatini U, Spalletta G. 2009. Aging of subcortical nuclei: microstructural, mineral-

ization and atrophy modifications measured in vivo using MRI. *Neuroimage*. 48(1):29–36. doi: 10.1016/j.neuroimage.2009.06.035.

Corbetta M, Shulman GL. 2002. Control of goal-directed and stimulus-driven attention in the brain. *Nat Rev Neurosci*. 3(3):201–215. doi: 10.1038/nrn755.

Chen T, Cai W, Ryali S, Supekar K, Menon V. 2016. Distinct global brain dynamics and spatiotemporal organization of the salience network. *PLoS Biol*. 14(6):e1002469.

Deco G, Jirsa VK, McIntosh AR. 2011. Emerging concepts for the dynamical organization of resting-state activity in the brain. *Nature Rev Neurosci*. 12(1):43–56. doi: 10.1038/nrn2961.

Desikan RS, Ségonne F, Fischl B, Quinn BT, Dickerson BC, Blacker D, Buckner RL, Dale AM, Maguire RP, Hyman BT *et al*. 2006. An automated labeling system for subdividing the human cerebral cortex on MRI scans into gyral based regions of interest. *Neuroimage*. 31(3):968–980. doi: 10.1016/j.neuroimage.2006.01.021.

Dixon ML, Andrews-Hanna JR, Spreng RN, Irving ZC, Mills C, Girn M, Christoff K. 2017. Interactions between the default network and dorsal attention network vary across default subsystems, time, and cognitive states. *Neuroimage*. 147:632–649. doi: 10.1016/j.neuroimage.2016.12.073.

Emer J. Hughes, Jacqueline Bond, Patricia Svrckova, Antonis Makropoulos, Gareth Ball, David J. Sharp, A. David Edwards, Joeseph V. Hajnal, Serena J. Counsell. 2012. Regional changes in thalamic shape and volume with increasing age. *Neuroimage*. 63(3):1134–1142.

Ferreira LK, Busatto GF. 2013. Resting-state functional connectivity in normal brain aging. *Neurosci Biobehav Rev*. 37(3):384–400. doi: 10.1016/j.neubiorev.2013.01.017.

Ferreira LK, Regina ACB, Kovacevic N, Martin MDGM, Santos PP, Carneiro CDG, Kerr DS, Jr EA, McIntosh AR, Busatto GF. 2016. Aging effects on whole-brain functional connectivity in adults free of cognitive and psychiatric disorders. *Cereb Cortex*. 26(9):3851–3865. doi: 10.1093/cercor/bhv190.

Fox MD, Corbetta M, Snyder AZ, Vincent JL, Raichle ME. 2006. Spontaneous neuronal activity distinguishes human dorsal and ventral attention systems. *Proc Natl Acad Sci USA*. 103(26):10046–10051. doi: 10.1073/pnas.0604187103.

Fransson P. 2005. Spontaneous low-frequency BOLD signal fluctuations: an fMRI investigation of the resting-state default mode of brain function hypothesis. *Hum Brain Mapp*. 26(1):15–29. doi: 10.1002/hbm.20113.

Geerligs L, Rubinov M, Tyler LK, Brayne C, Bullmore ET, Calder AC, Henson RN. 2015. State and trait components of functional connectivity: individual differences vary with mental state. *J Neurosci*. 35(41):13949–13961. doi: 10.1523/JNEUROSCI.1324-15.2015.

Geweke J. 1982. Measurement of linear dependence and feedback between multiple time series. *J Am Stat Assoc*. 77(378):304–313.

Geweke J. 1984. Measures of conditional linear dependence and feedback between time series. *J Am Stat Assoc*. 79:907–915.

Goldstone A, Mayhew SD, Hale JR, Wilson RS, Bagshaw AP. 2018. Thalamic functional connectivity and its association with behavioral performance in older age. *Brain Behav*. 8(4):1–17.

Goulden N, Khusnulina A, Davis NJ, Bracewell RM, Bokde AL, McNulty JP, Mullins PG. 2014. The salience network is responsible for switching between the default mode network and the central executive network: replication from DCM. *Neuroimage*. 99:180–190. doi: 10.1016/j.neuroimage.2014.05.052.

Granger CW. 1969. Investigating causal relations by econometric models and cross-spectral methods. Econometrica. *journal of the Econometric Society*. 424–438.

Grinband J, Steffener J, Razlighi QR, Stern Y. 2017. BOLD neurovascular coupling does not change significantly with normal aging. *Hum Brain Mapp*. 38(7):3538–3551.

Hwang K, Bertolero MA, Liu WB, D'Esposito M. 2017. The human thalamus is an integrative hub for functional brain networks. *J Neurosci*. 37(23):5594–5607. doi: 10.1523/jneurosci.0067-17.2017.

King BR, Van Ruitenbeek P, Leunissen I, Cuypers K, Heise KF, Santos Monteiro T, Hermans L, Levin O, Albouy G, Mantini D. 2018. Age-related declines in motor performance are associated with decreased segregation of large-scale resting state brain networks. *Cereb Cortex*. 28(12):4390–4402.

Li SC, Lindenberger U, Sikström S. 2001. Aging cognition: from neuromodulation to representation. *Trends Cogn Sci*. 5:479–486. doi: 10.1016/S1364-6613(00)01769-1.

Li JM, Bentley WJ, Snyder LH. 2015. Functional connectivity arises from a slow rhythmic mechanism. *Proc Natl Acad Sci*. 112(19):E2527–E2535.

Llinás RR, Ribary U, Jeanmonod D, Kronberg E, Mitra PP. 1999. Thalamocortical dysrhythmia: a neurological and neuropsychiatric syndrome characterized by magnetoencephalography. *Proc Natl Acad Sci USA*. 96(26):15222–15227. doi: 10.1073/pnas.96.26.15222.

McFarland NR, Haber SN. 2002. Thalamic relay nuclei of the basal ganglia form both reciprocal and nonreciprocal cortical connections, linking multiple frontal cortical areas. *J Neurosci*. 22(18):8117–8132.

Menon V, Uddin LQ. 2010. Saliency, switching, attention and control: a network model of insula function. *Brain Struct Funct*. 214:655–667. doi: 10.1007/s00429-010-0262-0.

Naik S, Banerjee A, Bapi RS, Deco G, Roy D. 2017. Metastability in senescence. *Trends Cogn Sci*. 21(7):509–521.

Ng KK, Lo JC, Lim JKW, Chee MWL, Zhou J. 2016. Reduced functional segregation between the default mode network and the executive control network in healthy older adults: a longitudinal study. *Neuroimage*. 133:321–330. doi: 10.1016/j.neuroimage.2016.03.029.

Obeso JA, Rodríguez-Oroz MC, Benitez-Temino B, Blesa FJ, Guridi J, Marin C, Rodriguez M. 2008. Functional organization of the basal ganglia: therapeutic implications for Parkinson's disease. *Mov Disord*. 23(S3):S548–S559.

Raichle ME. 2015. The Brain's default mode network. *Annu Rev Neurosci*. 38(1):433–447. doi: 10.1146/annurev-neuro-071013-014030.

Rangaprakash D, Wu GR, Marinazzo D, Hu X, Deshpande G. 2018. Hemodynamic response function (HRF) variability confounds resting-state fMRI functional connectivity. *Magn Reson Med*. 80(4):1697–1713.

Reid AT, Headley DB, Mill RD, Sanchez-Romero R, Uddin LQ, Marinazzo D, Lurie DL, Valdés-Sosa PA, José Hanson S, Biswal B *et al*. 2019. Advancing functional connectivity research from association to causation. *Nat Neurosci*. 22(11):1751–1760.

Reuter-Lorenz PA. 2002. New visions of the aging mind and brain für mehr Artikel. *Trends Cogn Sci*. 6(9):394–400. doi: 10.1016/S1364-6613(02)01957-5.

Sahoo B, Pathak A, Deco G, Banerjee A, Roy D. 2020. Lifespan associated global patterns of coherent neural communication. *Neuroimage*. 216:116824.

Sakaki M, Yoo HJ, Nga L, Lee TH, Thayer JF, Mather M. 2016. Heart rate variability is associated with amygdala functional

connectivity with MPFC across younger and older adults. *Neuroimage*. 139:44–52. doi: 10.1016/j.neuroimage.2016.05.076.

Schirner M, Rothmeier S, Jirsa VK, McIntosh AR, Ritter P. 2015. An automated pipeline for constructing personalized virtual brains from multimodal neuroimaging data. *Neuroimage*. 117:343–357. doi: 10.1016/j.neuroimage.2015.03.055.

Seidler RD, Bernard JA, Burutolu TB, Fling BW, Gordon MT, Gwin JT, Kwak Y, Lipps DB. 2010. Motor control and aging: links to age-related brain structural, functional, and biochemical effects. *Neurosci Biobehav Rev*. 34(5):721–733. doi: 10.1016/j.neubiorev.2009.10.005.

Serrien DJ, Ivry RB, Swinnen SP. 2007. The missing link between action and cognition. *Prog Neurobiol*. 82(2):95–107. doi: 10.1016/j.pneurobio.2007.02.003.

Sherman SM, Guillery RW. 2002. The role of the thalamus in the flow of information to the cortex. *Philos Trans R Soc Lond B Biol Sci*. 357(1428):1695–1708.

Smith SM, Fox PT, Miller KL, Glahn DC, Fox PM, Mackay CE, Filippini N, Watkins KE, Toro R, Laird AR *et al*. 2009. Correspondence of the brain's functional architecture during activation and rest. *Proc Natl Acad Sci USA*. 106(31):13040–13045. doi: 10.1073/pnas.0905267106.

Spreng RN, Turner GR. 2019. The shifting architecture of cognition and brain function in older adulthood. *Perspectives on Psychological Science*. 14(4):523–542.

Sridharan D, Levitin DJ, Menon V. 2008. A critical role for the right fronto-insular cortex in switching between central-executive and default-mode networks. *Proc Natl Acad Sci USA*. 105(34):12569–12574. doi: 10.1073/pnas.0800005105.

Stramaglia S, Cortes JM, Marinazzo D. 2014. Synergy and redundancy in the Granger causal analysis of dynamical networks. *New J Phys*. 16(10):105003.

Tang L, Ge Y, Sodickson DK, Miles L, Zhou Y, Reaume J, Grossman RI. 2011. Thalamic resting-state functional networks: disruption in patients with mild traumatic brain injury. *Radiology*. 260(3):831–840. doi: 10.1148/radiol.11110014.

Uddin LQ, Iacoboni M, Lange C, Keenan JP. 2007. The self and social cognition: the role of cortical midline structures and mirror neurons. *Trends Cogn Sci*. 11(4):153–157.

Uddin LQ, Supekar KS, Ryali S, Menon V. 2011. Dynamic reconfiguration of structural and functional connectivity across core neurocognitive brain networks with development. *J Neurosci*. 31(50):18578–18589.

Uddin LQ. 2015. Salience processing and insular cortical function and dysfunction. *Nat Rev Neurosci*. 16(1):55–61. doi: 10.1038/nrn3857.

Uddin LQ, Kelly AMC, Biswal BB, Castellanos FX, Milham MP. 2009. Functional connectivity of default mode network components: correlation, anticorrelation, and causality. *Hum Brain Mapp*. 30(2):625–637. doi: 10.1002/hbm.20531.

Uddin LQ, Yeo BT, Spreng RN. 2019. Towards a universal taxonomy of macro-scale functional human brain networks. *Brain Topogr*. 32(6):926–942.

Vanneste S, Song JJ, De Ridder D. 2018. Thalamocortical dysrhythmia detected by machine learning. *Nat Commun*. 9(1):1–13.

Vij SG, Nomi JS, Dajani DR, Uddin LQ. 2018. Evolution of spatial and temporal features of functional brain networks across the lifespan. *Neuroimage*. 173:498–508.

Walhovd KB, Fjell AM, Reinvang I, Lundervold A, Dale AM, Eilertsen DE, Quinn BT, Salat D, Makris N, Fischl B. 2005. Effects of age on volumes of cortex, white matter and subcortical structures. *Neurobiol Aging*. 26(9):1261–1270; discussion 1275-8. doi: 10.1016/j.neurobiolaging.2005.05.020.

Wang HLS, Rau CL, Li YM, Chen YP, Yu R. 2015. Disrupted thalamic resting-state functional networks in schizophrenia. *Frontiers in Behavioral Neuroscience*. 9(Feb):1–9. doi: 10.3389/fnbeh.2015.00045.

Woodward ND, Cascio CJ. 2015. Resting-state functional connectivity in psychiatric disorders. *JAMA Psychiat*. 72(8):743–744. doi: 10.1001/jamapsychiatry.2015.0484.

Xiao T, Zhang S, Lee LE, Chao HH, van Dyck C, Li CSR. 2018. Exploring age-related changes in resting state functional connectivity of the amygdala: from young to middle adulthood. *Front Aging Neurosci*. 10(209):1–14.

Yuen NHY, Osachoff N, Chen J. 2019. Intrinsic frequencies of the resting-state fMRI signal: the frequency dependence of functional connectivity and the effect of mode mixing. *Front Neurosci*. 13:900.

Zheng F, Cui D, Zhang L, Zhang S, Zhao Y, Liu X, Liu C, Li Z, Zhang D, Shi L *et al*. 2018. The volume of hippocampal subfields in relation to decline of memory recall across the adult lifespan. *Front Aging Neurosci*. 10(320):1–10.